Journal of Molecular Spectroscopy 351 (2018) 39–48

Contents lists available at ScienceDirect

Journal of Molecular Spectroscopy

journal homepage: www.elsevier.com/locate/jms

The 103–360 GHz rotational spectrum of benzonitrile, the first interstellar benzene derivative detected by radioastronomy

Maria A. Zdanovskaia [a], Brian J. Esselman [a], Hunter S. Lau [a], Desiree M. Bates [a], R. Claude Woods [a,*], Robert J. McMahon [a,*], Zbigniew Kisiel [b,*]

[a] Department of Chemistry, University of Wisconsin–Madison, Madison, WI 53706, USA
[b] Institute of Physics, Polish Academy of Sciences, Al. Lotników 32/46, 02-668 Warszawa, Poland

ARTICLE INFO

Article history:
Received 18 May 2018
In revised form 26 June 2018
Accepted 27 June 2018
Available online 28 June 2018

Keywords:
Millimeter-wave
Rotational spectroscopy
Coriolis coupling
Nominal interstate transitions
Interstellar molecule
Astrochemistry

ABSTRACT

Recently, several cm-wave transitions of benzonitrile have been detected in the interstellar medium (TMC-1). In this work, the mm-wave spectrum of benzonitrile (C_6H_5CN, C_{2v}, μ_a = 4.5 D), a planar asymmetric rotor molecule, is reported in the 103–360 GHz frequency region. Over 3000 rotational transitions have been newly measured for the ground state and were combined with previous data in a global fit, which allows predictions of both low-temperature hyperfine resolved and high-frequency unresolved rotational spectra. Rotational transitions in the lowest fundamentals, v_{22} and v_{33} (141 and 163 cm^{-1}, respectively), have been observed for the first time, and were complemented by identification of several nominal interstate transitions resulting from strong interstate mixing. Application of a two-state, Coriolis-coupled model accounted, to within experimental precision, for many identified interstate perturbations resulting in $\Delta E_{22,33}$ = 19.108185(7) cm^{-1} and $|\zeta^a_{22,33}|$ = 0.841(7). This study provides insight into the generic problem affecting the lowest excited vibrational states of this molecular class and describes the techniques allowing its successful analysis. The new data provide the foundation for future remote detection applications of benzonitrile.

© 2018 Elsevier Inc. All rights reserved.

1. Introduction

Since the reported infrared detection of benzene in the interstellar medium (ISM) by Cernicharo et al. [1], there has been increased motivation to detect analogous aromatic molecules more reliably by radioastronomy [2,3]. Two small aromatic molecules, cyclopropenylidene [4,5] and cyclopropenone[6], have already been detected in the ISM. Due to its strong dipole moment (μ_a = 4.5 D) [7], being a derivative of benzene, and the fact that numerous nitriles have been detected in the ISM [8], benzonitrile (C_6H_5CN, depicted in Fig. 1) provided a very attractive target for direct detection in the ISM by means of its rotational transitions and radioastronomy.

Indeed, benzonitrile has been detected in the ISM [9,10] by observation of nine hyperfine-resolved rotational transitions in Taurus Molecular Cloud 1 (TMC-1) [11] from 18 to 23 GHz using the Green Bank Telescope. These astronomical observations in the cm-wave region motivate a refinement of the benzonitrile spectroscopic constants and an extension of the mm-wave broadband spectrum. Despite the availability of instruments that can observe mm-wave spectra, such as the Atacama Large Millimeter Array (ALMA), nearly all of the mm-wave data previously available for benzonitrile have been in a relatively narrow band of 152–160 GHz [12] and no astronomical searches in the mm-wave region have been reported.

Benzonitrile is a prolate (κ = −0.85) asymmetric rotor with C_{2v} symmetry and its substantial dipole moment along its *a*-inertial axis results in intense ^{a}R-type absorptions. The rotational spectrum of benzonitrile has been studied extensively in the cm-wave region (1–30 GHz) [7,9,13–18]. Erlandsson and Lide independently published the first rotational spectral analyses in 1954 [13,14]. Bak et al. later published infrared (IR) and cm-wave analyses of benzonitrile, producing a complete substitution structure based on data for the parent isotopologue and all possible mono-substituted isotopologues [15,19]. This structure was refined by Casado et al. with the addition of several Q-branch transitions for most of the mono-substituted isotopologues [16]. Green and Harrison refined the analysis of the experimental IR spectrum, accounting also for the lowest wavenumber modes [20], while Csaszar and Fogarasi carried out a computed harmonic force field

* Corresponding authors.
E-mail addresses: rcwoods@wisc.edu (R.C. Woods), robert.mcmahon@wisc.edu (R.J. McMahon), kisiel@ifpan.edu.pl (Z. Kisiel).

https://doi.org/10.1016/j.jms.2018.06.004
0022-2852/© 2018 Elsevier Inc. All rights reserved.

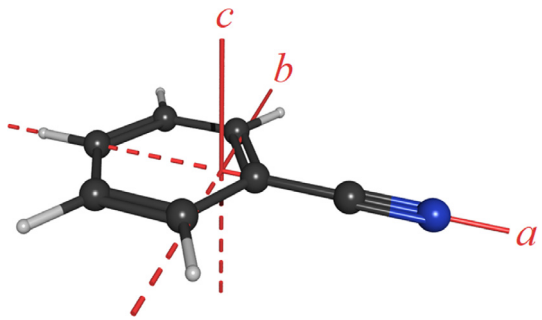

Fig. 1. Benzonitrile structure with principal rotation axes.

analysis [21]. Wlodarczak et al. extended the observed spectroscopic transitions into the mm-wave region (up to 160 GHz), providing a substantial improvement in the determination of the centrifugal distortion constants [12]. The rotational constants, hyperfine coupling constants, and dipole moment were well-determined by supersonic expansion Fourier-transform microwave (FTMW) spectroscopy [7]. In the course of the study by Dahmen et al., the rotational constants for the heavy isotopologues of benzonitrile were refined, resulting in an updated substitution structure [22]. Most recently, Rudolph et al. determined the semi-experimental equilibrium structure of benzonitrile using B3LYP-calculated vibration-rotation interaction (α_i) constants and the previously published rotational constants for ten isotopologues [23].

Parallel to the laboratory spectroscopic work, several authors have suggested mechanisms of formation and postulated the presence of benzonitrile in extra-terrestrial bodies and the ISM [24–28]. Khare et al. demonstrated that an electric discharge of a mixture of methane, ammonia, and water generated benzonitrile at a range of temperatures (150–600 °C) [24]. While not directly analogous to the ISM, these experiments were designed to show that complex organic molecules could be generated from simple gases under conditions observed in the Jovian planets. Balucani et al. explored the formation of benzonitrile and a hydrogen atom using a crossed molecular beam collision of a cyano radical and benzene, concluding that the barrierless reaction was favorable by 95 kJ/mol [25]. Woods et al. suggested that, in the proto-planetary nebula CRL 618, the concentration of benzonitrile, generated primarily *via* the reaction between benzene and cyano radical, was similar to that of benzene [26]. Additionally, Woon explored this reaction computationally (MP2 and B3LYP) and concluded that benzonitrile formation dominated the chemistry of benzene and cyano radical across a wide range of temperatures and pressures relevant for Titan's atmosphere [27]. Most recently, Parker et al. observed benzonitrile after mixing nitrosobenzene and vinyl cyanide in a pyrolytic reactor [28]. They proposed that phenyl radical is generated *in situ* along with cyanovinyl radical, which subsequently decomposes to the cyano radical and reacts with the phenyl radical to form benzonitrile. Thus, benzonitrile has been a clear target for radioastronomical detection due to its favorable dipole and ability to be generated from cyano radical [29] and benzene, [1,30,31] which have both been detected in the ISM.

In the current study, we performed new measurements of the rotational spectrum of benzonitrile in the 103–360 GHz frequency region. Extensive measurements were performed for the ground state, and for the two lowest energy vibrational states. The rotational transitions in these two states have been assigned for the first time and were found to be only partially amenable to a single-state model. As has been observed with other single-ring aromatic compounds and larger polycyclic aromatic hydrocarbons (PAHs) [32–34], these two lowest energy vibrational states are strongly coupled. In the case of quinoline [34], phenylacetylene [32], and the current work, transitions in these two states were fitted with a two-state model that ultimately accounted for all observable transitions to within the measurement accuracy. The coupling of the two lowest-energy vibrational modes appears to be the norm for these aromatic molecules and should be considered when investigating these species and preparing for their radioastronomical observations.

2. Experimental methods

Commercially available samples of benzonitrile were used without further purification for all measurements. The 103–136 GHz (low) and 185–207 GHz (mid) portions of the spectrum were recorded with the millimeter-wave spectrometer in Warsaw that uses source modulation and second derivative detection. The low-frequency segment was recorded using a synthesizer-driven 12 × VDI multiplier source [35] and the mid-frequency range was collected using a phase-locked direct generation BWO source [32]. Both spectra were acquired at room temperature and 5 mTorr sample pressure. The 250–360 GHz (high) spectrum was collected on a broadband spectrometer in Madison with benzonitrile pressures of 2–6 mTorr [33]. The high-frequency benzonitrile spectrum was collected at room temperature and at −50 °C, the latter to minimize the abundance and resulting intensity of transitions in high-energy vibrational satellites.

The spectra were combined into a single broadband spectrum using the Assignment and Analysis of Broadband Spectra (AABS) software [36,37]. In addition to the AABS suite, the PIFORM, PISLIN, PMIXC, PLANM, and AC programs were used for spectral viewing and analysis [38,39]. Least-squares fits and spectral predictions were carried out using Pickett's SPFIT/SPCAT [40]. In the fits, we assumed uniform frequency measurement uncertainty of 50 kHz for all present measurements, and uncertainties specified by the respective authors for the literature data. In the case where such a value was not given (Ref. [18]) we assumed an uncertainty of 5 kHz, which resulted in weighted, root mean square (rms) deviation for this subset that was similar to those for the other literature data subsets.

3. Computational methods

The CCSD/ANO1 [41] geometry optimization and VPT2 anharmonic frequency calculations were performed using CFOUR 2.0 [42]. The geometry optimization utilized analytic gradients [43,44] with the frozen core approximation. Numerical differentiation of the analytic second derivatives at displaced points was used to obtain cubic force constants [45,46], which allowed calculation of vibration-rotation interaction constants (α_i values). A geometry optimization using OPT = tight with an ultrafine grid and anharmonic vibration-rotation calculations at the B3LYP/6-311+G(2d,p) level were conducted in Gaussian 09 [47] *via* the WebMO interface [48]. Output files of computational work are provided in the Supplementary Material. The two levels of anharmonic computations were designed to test a stepwise computing approach, since the B3LYP calculation corresponded to 246 basis functions and the much lengthier CCSD calculation (two months on a multi-node cluster) was based on 315 basis functions. Centrifugal distortion constants were also predicted by the B3LYP and CCSD calculations. Unfortunately, the quartic force constants in the CCSD calculation were poorly determined, resulting in unreasonable anharmonic frequencies for many states. These problems affected primarily the highest wavenumber modes. Though not as drastic, the low energy vibrational modes also had unreasonable anharmonic energy differences. The lowest-order vibration-rotation (α_i)

changes in rotational constants and centrifugal distortion constants, however, require only a cubic anharmonic contribution, and those were less affected than the correction from harmonic to fundamental frequencies, as evidenced by their close agreement to empirically determined values.

4. Analysis of rotational spectra

4.1. Ground state

The benzonitrile spectrum in the 103–136 GHz, 185–206.5 GHz, and 250–360 GHz ranges is fairly dense and features multiple vibrational satellites. While the assignment, measurement, and least-squares fitting of three states are discussed in this work, tentative assignments have been made also for three more fundamentals and several additional overtones and combination bands. A sample region of the experimental spectrum at the onset of the submillimeter region is shown in Fig. 2, with an accompanying stick spectrum for the ground state, v_{22}, and v_{33}.

Throughout our observational range, the most intense transitions for benzonitrile and its observed vibrational states belong to $n = 2$, type-II$^+$, $^aR_{0,1}$ bands [49,50]. In such series, the values of J decrease, and those of K_a increase on moving away from the lead line in the band. Within a given band, the leading line is at lowest frequency, and consists of two degenerate transitions for the same value of J: one for $K_a = 0$, the other for $K_a = 1$, but with the same value of K_c. The quantum numbers for the energy levels of the two degenerate transitions are, therefore, connected by the conditions $K_a + K_c = J$ and $K_a + K_c = J + 1$, respectively, and notation K_a^J and K_a^{J+1} is used below for brevity. At higher values of K_a these transitions lose the degeneracy, while at even greater values of K_a the degeneracy returns but the two degenerate components are now for same value of K_a. For the ground state lines in the region of Fig. 2, these two transition points between degeneracy and splitting are at $K_a = 14^J$, 15^{J+1} and above $K_a = 25$, respectively. The intensities of the measured rotational transitions are affected by nuclear spin statistical weights resulting from the presence of two pairs of symmetry equivalent protons in the phenyl ring of benzonitrile. The statistics are not immediately apparent in the spectrum, since many lines are degenerate spectroscopic doublets, but are readily visible for close pairs of lines with the same value of K_c. The statistics are 5:3 for even:odd symmetry of the vibronic wavefunction in the ground state, and reverse to 3:5 for B-symmetry states, in a situation identical to that described in more detail for phenylacetylene [32]. The R-branch bands are separated by ~2400 MHz (approximately $2C$), but are interspersed with many lower J, higher K_a transitions, which do not group into easily discernible patterns.

For the vibrational ground state, we measured over 3000 new absorptions, all belonging to $^aR_{0,1}$ branch transitions, ranging in J'' from 37 to 147 and in K_a from 0 to 68. The present measurements were fitted in a single global fit combining previous hyperfine-resolved and hyperfine unresolved literature data. The resulting spectroscopic constants in Watson's asymmetric rotor Hamiltonian (A-reduction, I^r representation) [51] are reported in Table 1. The current scope and the extent of expansion of the rotational data set are apparent from the diagram in Fig. 3. The first two columns of Table 1 report previous fits based either only on hyperfine resolved supersonic expansion measurements [7,9] or only on hyperfine unresolved frequencies [12]. Even though we did not make any hyperfine resolved measurements, we find that the precision in the nuclear quadrupole splitting constants χ_{aa} and χ_{bb} for the nitrogen nucleus is improved by a factor of three. This provides a corresponding increase in prediction accuracy for cm-wave transition in low temperature astrophysical environments.

Similarly, even though we did not measure any Q-branch transitions, which are most effective in determining the purely K dependent Hamiltonian parameters, we find that the precision in rotational constant A_0 and in the centrifugal distortion constant Δ_K has been improved by well over an order of magnitude. The experimentally determined spectroscopic parameters are found to be in good agreement with the two anharmonic calculations. It is difficult to choose between the two sets of computed results except, perhaps, for poorer B_0 from the CCSD calculation. Nevertheless, the performance of both computations concerning the ground state rotational constants is equally impressive, and the corrections $A_e - A_0$ between ground state to equilibrium are consistent and close to 42 MHz; $B_e - B_0$ and $C_e - C_0$ are near 6 MHz. The computations overestimate the observed inertial defect, Δ_i = 0.080084 (3) uÅ^2, as was found in ref [23], where it was also shown that further improvement requires electron mass contribution corrections.

We have been able to determine all but one sextic centrifugal distortion constants, and these are in excellent agreement with the values computed from the anharmonic force field. A comparison of sextic constants for a molecule of this size and is quite rare, as benchmark studies of sextic constant computations have only been made for molecules with a few atoms. Interestingly, we have not been able to determine the sextic centrifugal distortion constant

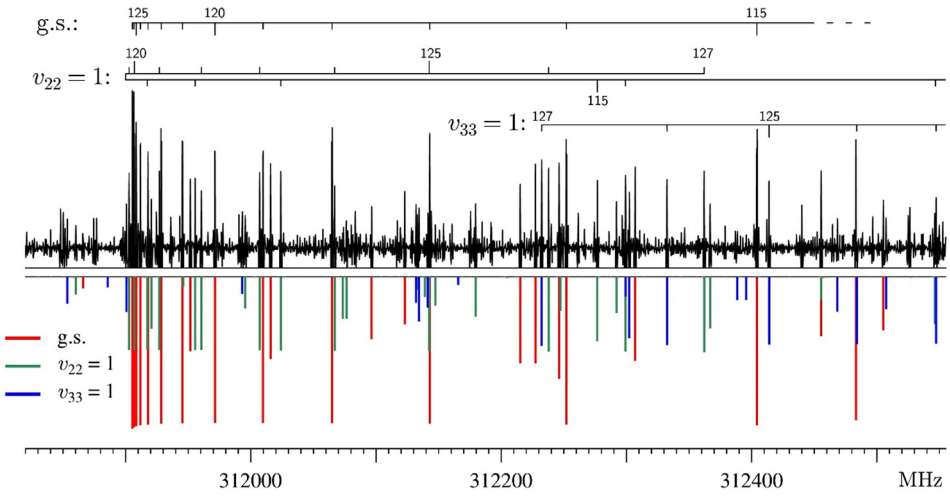

Fig. 2. Benzonitrile rotational spectrum from 311,900 to 312,600 MHz (top) and stick spectrum of the ground vibrational state, v_{22}, and v_{33} transitions (bottom). The strongest transitions belong to the $n = 2$, type-II$^+$ bands, indicated above the spectrum, where values of J'' are marked. Many yet-to-be analyzed transitions belonging to other vibrational satellites are visible.

Table 1
Experimental and computational spectroscopic constants for the ground vibrational state of benzonitrile.

	Wlodarczak [12][a]	McGuire [9][b]	Current work[c]	B3LYP[d]	CCSD[e]
A_0 (MHz)	5655.2647(20)	5655.26522(59)	5655.265371(75)	5650.12	5661.67
B_0 (MHz)	1546.87589(16)	1546.875836(63)	1546.8757804(76)	1546.59	1544.99
C_0 (MHz)	1214.40434(14)	1214.404061(48)	1214.4040772(67)	1213.97	1213.50
Δ_J (kHz)	0.045287(22)	0.04563(28)	0.0452653(27)	0.04358	0.04316
Δ_{JK} (kHz)	0.93268(29)	0.9333(24)	0.937906(27)	0.8790	0.8886
Δ_K (kHz)	0.3175(112)	0.272(64)	0.24234(77)	0.2795	0.2570
δ_J (kHz)	0.0110056(51)	0.01111(16)	0.01101589(73)	0.01056	0.01047
δ_K (kHz)	0.60649(24)	0.6136(73)	0.609088(74)	0.5690	0.5743
Φ_J (Hz)			0.00000051(22)	0.000000765	
Φ_{JK} (Hz)			0.0015435(46)	0.00133	
Φ_{KJ} (Hz)	−0.00552(15)		−0.007849(17)	−0.00727	
Φ_K (Hz)	0.200(24)		[0.]	0.00624	
ϕ_J (Hz)			0.000001412(38)	0.00000104	
ϕ_{JK} (Hz)			0.0007431(30)	0.000677	
ϕ_K (Hz)			0.007106(76)	0.00561	
L_J (μHz)			0.0000585(56)		
L_{JJK} (μHz)			−0.002085(52)		
L_{KKJ} (μHz)			−0.0428(18)		
L_K (μHz)			4.468(90)		
χ_{aa} (MHz)		−4.23797(89)	−4.23755(27)		
χ_{bb} (MHz)		2.28907(118)	2.28872(38)		
Δ_i (uÅ^2)[f]	0.080007(67)	0.080099(23)	0.080084(3)	0.0873	0.0924
N[g]	166	146	4073		
σ_{fit} (MHz)		0.00130	0.0248		
σ_{rms}[h]		0.622	0.520		

[a] Fit to previous hyperfine unresolved data up to 160 GHz.
[b] Fit to hyperfine resolved data from supersonic expansion measurements.
[c] Global fit to the present mm-wave measurements and the available literature data [7,9,12,16,18].
[d] Evaluated with the 6-311+G(2d,p) basis set.
[e] Evaluated with the ANO1 basis set.
[f] Inertial defect, $\Delta_i = I_c - I_a - I_b$.
[g] Number of fitted transition frequencies.
[h] Unitless deviation of the weighted fit.

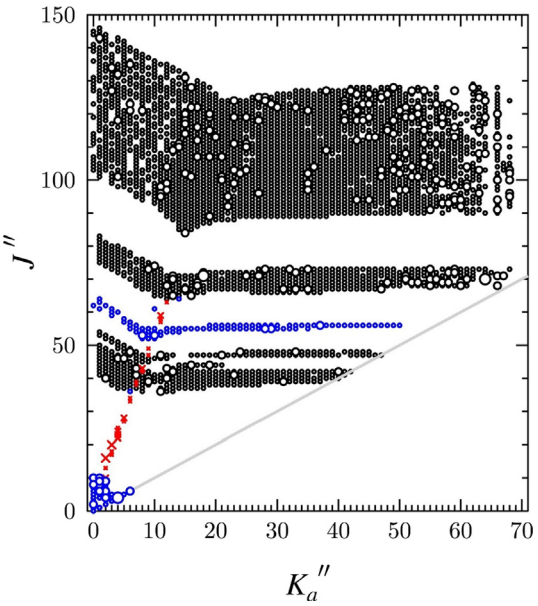

Fig. 3. Data distribution plot for the global fit of combined spectroscopic data for the vibrational ground state of benzonitrile. The size of the plotted symbol is proportional to the value of $|(f_{obs.} - f_{calc.})/\delta f|$, where δf is frequency measurement uncertainty, and all values are smaller than 3. Black symbols denote data from the present work, colored symbols mark literature [7,9,12,16,18]. Circles mark $^aR_{0,1}$ branch transitions, and crosses identify literature Q-branch transitions and a single P-branch transition. (For interpretation of the references to color in this figure legend, the reader is referred to the web version of this article.)

Φ_K, while it was necessary to use the related, higher-order constant L_K. This may be the first indication that at the very high K_a values of up to 68 reached by the present data there is some interaction with rotational levels of vibrational states above the ground state.

4.2. The lowest vibrational states, $v_{22} = 1$ and $v_{33} = 1$

The first excited vibrational states of the two lowest fundamental modes, v_{22} (141 cm^{-1}, B_1 symmetry) [20,21] and v_{33} (163 cm^{-1}, B_2 symmetry) [20,21], are sufficiently close in energy that their rotational spectra display the effects of a strong vibration-rotation interaction. These two low-frequency vibrations are mutually perpendicular bends associated with the nitrile functional group (R—C≡N). The v_{22} normal mode is the out-of-plane bend of the nitrile with respect to the aromatic ring, while v_{33} is the corresponding in-plane bend. Fig. 4 shows the complex vibrational energy level pattern for this molecule; eighteen excited vibrational states are expected to be present below 600 cm^{-1}. All of these states are expected to give rise to measurable rotational transitions in the room temperature rotational spectrum. Even though the analysis of the $2v_{22}$, $v_{22}+v_{33}$, and $2v_{33}$ triad and of the fundamentals v_{21}, v_{15}, and v_{12} is ongoing, it is not yet sufficiently mature for inclusion in the present work. Tables of all fundamental modes, their symmetries, harmonic frequencies, and infrared intensities calculated at the B3LYP/6-311+G(2d,p) and CCSD/ANO1 levels of theory are provided in the Supplementary Material.

The rotational transition patterns for both v_{22} and v_{33} are dominated by the same type-II$^+$ bands, as seen in Fig. 2, and show similar degeneracy behavior to that of the ground state. Since

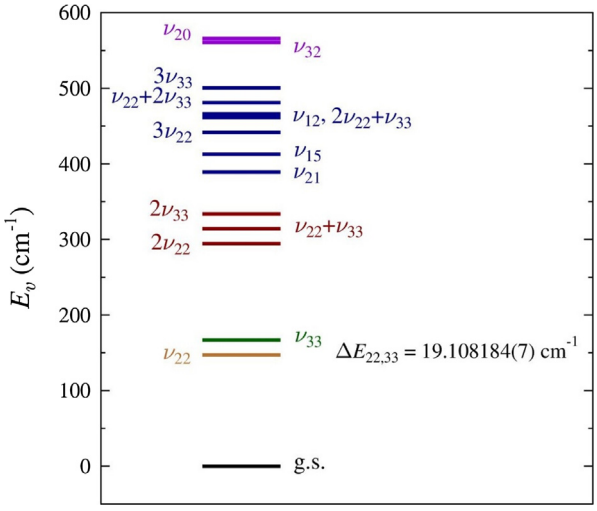

Fig. 4. The vibrational energy levels of benzonitrile below 600 cm^{-1}, drawn from harmonic values of the CCSD/ANO1 calculation. Four combination levels above 530 cm^{-1} involving ν_{15} and ν_{21} modes have been omitted for clarity. The denoted ν_{33}–ν_{22} energy difference results from the perturbation analysis of the present work.

separation between successive bands is also determined by 2C and the vibrational changes in this rotational constant are small (less than 2 MHz) these excited state bands turn out to be close in frequency to the corresponding bands for the ground state. The distribution of lines in type-II$^+$ bands, however, is critically dependent on the effective inertial defect in each state, and in both cases this is significantly different from that in the ground state. The result is a much broader line distribution for ν_{33}, and an equally broad band structure for ν_{22}, but one that is characterized by a turnaround (see Fig. 2).

Analysis of rotational transitions in the two states commenced with assignment of low K_a lines in low- and mid-frequency ranges, and two separate single-state asymmetric rotor fits. Anharmonic calculations of vibrational changes in rotational constants were used for initial predictions, while starting values of centrifugal distortion constants were set to the experimentally determined values of the ground state. This allowed confident assignment of the lowest frequency, lowest K_a transitions, up to the point when satisfactory deviations of fit could not be reached with single state fits even on significant expansion in the number of fitted centrifugal distortion constants. At the same time, the values of many such constants began to significantly diverge relative to those of the ground state, but in opposite directions for the two states, in a clear signature of interstate coupling. Setting up a suitable two-state fit required determination of the type of interaction taking place. Since ν_{22} and ν_{33} belong to B_1 and B_2 irreducible representations, respectively, of the C_{2v} symmetry point group of the benzonitrile molecule, this excluded the possibility of a Fermi resonance. Coriolis-coupling would, however, be allowed along the inertial axis whose angular momentum component transforms like the irreducible representation of the product $B_1 \otimes B_2 = A_2$. This is the a-inertial axis and coupling between first excited states of the two modes is directly proportional to the value of the relevant Coriolis coupling constant, in this case $\zeta^a_{22,33}$. The corresponding spectroscopic constant, G_a, is directly related to $\zeta^a_{22,33}$ by

$$G_a = \frac{\omega_{22} + \omega_{33}}{\sqrt{\omega_{22} \times \omega_{33}}} \zeta^a_{22,33} A, \quad (1)$$

where ω_{22} and ω_{33} are the harmonic frequencies for the two modes, and A is normally identified with the rotational constant A_0, since this is a harmonic level expression accounting for changes relative to the ground state. The key coupling parameters for setting up the calculation were thus the vibrational energy difference, ΔE, between the two states and the first-order Coriolis coupling coefficient, G_a, which were both estimated on the basis of the computations. Even prior to refining the fit, it was possible to see with Loomis-Wood type techniques built into the AABS package [36] that there were a considerable number of local, level-crossing resonances affecting rotational transition frequencies. Matching such resonances in the two vibrational states (as described below) allowed rapid refinement of the values of the interstate coupling terms. It turned out that, in addition to G_a, only three other coupling coefficients (G^J_a, F_{bc}, and F^K_{bc}) were required in an expansion of the coupling Hamiltonian described previously [52]. The final analysis requires only these four parameters and ΔE in order to describe all of the observed effects of the interstate interactions down to experimental accuracy. The resulting values of spectroscopic constants from the two-state least squares fit of the measured transitions for the ν_{22} and ν_{33} dyad are listed in Table 2 and distribution plots of obs. – calc. frequencies from the final fit are shown in Fig. 5.

The excited vibrational state transitions in the mm-wave spectrum are, as for the ground state, observable only for the $^aR_{0,1}$ selection rule and were measured up to $K_a = 47$. Transitions for higher values of K_a were also assignable and consistent with the final fit. Nevertheless, the upper cutoff in K_a was imposed in order to avoid introducing instabilities into the data set from very weak transitions where frequency measurements became considerably more prone to errors from blending with other lines. The final data set includes around 3000 independent lines for each vibrational state; deviations of fit are less than 40 kHz both for the overall coupled state fit and for the data subsets for each vibrational state. These values show that the frequency measurement error of 50 kHz assumed in weighted fits involving present data is somewhat overestimated. Table 2 allows a direct comparison of the excited state constants against those for the ground state, showing minimal vibrational variation of centrifugal distortion constants. In fact, this small variation allowed us to use, as parameters of fit, six fewer high-order centrifugal distortion constants than in the ground state. All of the excited state quartic constants are within 3% of the ground state values, and the three best-determined sextic constants change within 21% relative to the ground state, all of which is indicative of very satisfactory decoupling of perturbation effects from centrifugal distortion.

The only apparent deficiency of the coupled fit is the poor determination of A_{22}, A_{33}, G_a and, as it turns out, also of F_{bc}. This is due to practically unit correlation between these four parameters and is similar to the situation encountered before for quinolone [34] and phenylacetylene [32]. The correlation matrix for these parameters is provided in the Supplementary Material. The measured transition set already determines the vibration-rotation energy level structure completely and the indeterminacies cannot be broken by introducing transitions with different selection rules, even such as far-infrared vibration-rotation transitions in the case of quinolone [34]. It is still possible, however, to reduce the number of intercorrelated parameters by fitting their suitable linear combinations [32,34], also listed in Table 2. In the present case, we find that $(A_{22} + A_{33})/2$ is determined very precisely, while the poor accuracy in the separate A_{22} and A_{33} values arises from the practically indeterminate $(A_{22} - A_{33})/2$. Complete data files and results of the fits are available in the Supplementary Material.

4.2.1. Understanding the resonances

The two fundamentals exhibited the effects of both global and local perturbations. Fig. 6 illustrates a representative, broad, non-resonant global perturbation between ν_{22} and ν_{33}, for the $K_a = 9^J$ transition series. In the absence of perturbation, this type of plot

Table 2
Experimentally determined parameters for $v_{22} = 1$ and $v_{33} = 1$ excited vibrational states of benzonitrile compared to those for the ground state.

	g.s.	$v_{22} = 1$ (B_1, 141 cm^{-1}) [20,21]	$v_{33} = 1$ (B_2, 163 cm^{-1}) [20,21]
A_v (MHz)	5655.265371(75)	5654.5(20)	5654.8(20)
B_v (MHz)	1546.8757804(76)	1548.621160(52)	1549.725942(47)
C_v (MHz)	1214.4040772(67)	1216.238170(44)	1215.222889(52)
Δ_J (kHz)	0.0452653(27)	0.0459950(27)	0.0461715(27)
Δ_{JK} (kHz)	0.937906(27)	0.94708(40)	0.90714(40)
Δ_K (kHz)	0.24234(77)	[0.2423][a]	[0.2423][a]
δ_J (kHz)	0.01101589(73)	0.01108369(59)	0.01136762(49)
δ_K (kHz)	0.609088(74)	0.607315(93)	0.612108(91)
Φ_J (Hz)	0.00000051(22)	0.000001166(86)	0.000000675(89)
Φ_{JK} (Hz)	0.0015435(46)	0.0013917(22)	0.0016545(22)
Φ_{KJ} (Hz)	−0.007849(17)	−0.00619(12)	−0.00907(12)
ϕ_{JK} (Hz)	0.0007431(30)	0.0007493(41)	0.0006727(42)
ΔE (MHz)			572848.96(20)[b]
ΔE (cm^{-1})			19.108185(7)[b]
G_a (MHz)			9532.(62)[b]
G_a^J (MHz)			−0.004588(27)[b]
F_{bc} (MHz)			−0.411(39)[b]
F_{bc}^K (kHz)			−0.00981(44)[b]
$(A_{22} + A_{33})/2$ (MHz)			5654.61500(70)
$(A_{22} - A_{33})/2$ (MHz)			0.1(20)
N		3001	2933
σ (MHz)[c]		0.033680	0.037337

[a] Δ_K, along with all sextic and octic centrifugal distortion constants not listed explicitly, were fixed at the ground state values from Table 1.
[b] ΔE, G_a and F_{bc} parameters are for coupling with the $v_{22} = 1$ vibrational state, which is at lower energy.
[c] Deviations for the two vibrational state subsets: the overall standard deviation of the coupled fit to 5934 lines is 0.0356 MHz.

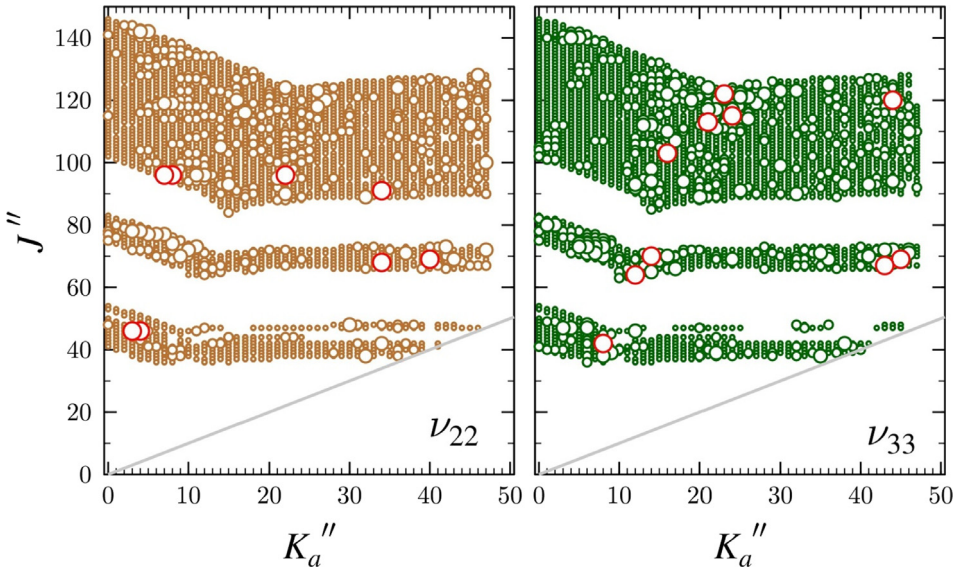

Fig. 5. Distribution plots of values of $|(f_{obs.} - f_{calc.})/\delta f|$ for the coupled fit of measured transitions in the two lowest excited vibrational states in benzonitrile. There are only a limited number of transitions with values of $|(f_{obs.} - f_{calc.})/\delta f| > 3$, and those are plotted in red, demonstrating that there is no systematic pattern of deviations from the assumed Hamiltonian. (For interpretation of the references to color in this figure legend, the reader is referred to the web version of this article.)

would be of relatively small amplitude, but this is considerably enhanced by the present Coriolis interaction.

The effective A rotational constants for the excited states would carry additional Coriolis contributions given by [32]:

$$A_{22} - A_0 = \frac{2A^2}{\omega_{22}} \left(\zeta^a_{22,33}\right)^2 \frac{3\omega_{22}^2 + \omega_{33}^2}{\omega_{22}^2 - \omega_{33}^2}, \quad (2)$$

$$A_{33} - A_0 = \frac{2A^2}{\omega_{33}} \left(\zeta^a_{22,33}\right)^2 \frac{3\omega_{33}^2 + \omega_{22}^2}{\omega_{33}^2 - \omega_{22}^2}, \quad (3)$$

which amplify the effects arising from molecular asymmetry, as seen in Fig. 6. The plots for the two states also display two examples of very sharp level-crossing resonances at $J > 100$. Efficient and unambiguous identification of such resonances requires suitable visualization techniques in order to guide measurements and fits. The most useful tools are Loomis-Wood and resonance plots, both built into the AABS package [36]. Loomis-Wood type plots align segments of recorded spectra on calculated frequencies of successive transitions of a given type. These plots allowed initial line assignments by following transition series for a selected value of K_a as a function of J. Transitions near the maxima of sharp resonances were

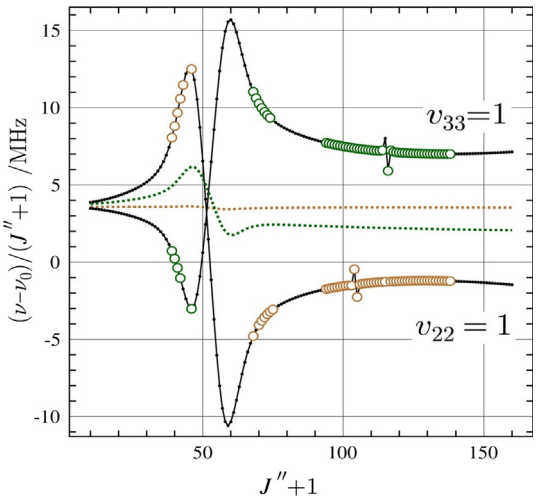

Fig. 6. Difference frequency plot for $K_a = 9^J$ rotational transition sequences in $v_{22} = 1$ (copper) and $v_{33} = 1$ (green) vibrational states, indicating the effect of the non-resonant part of the Coriolis perturbation between these two states. The plotted values are frequency differences between excited state transitions and their ground state counterparts, scaled by $(J'' + 1)$ in order to make the plots more horizontal. Measured transitions are represented by open circles, while dotted lines identify the much smaller asymmetry contribution responsible for reduction in the amplitude of the plot for $v_{33} = 1$. Two local perturbations are also visible at $J > 100$. (For interpretation of the references to color in this figure legend, the reader is referred to the web version of this article.)

more difficult to assign, and this was facilitated by means of resonance plots, as in the example in Fig. 7. In the implementation of the rotational Hamiltonian, the calculation of transition frequencies involves diagonalization of separate matrices for each value of J. For a given value of J, a simple resonance between two rotational energy levels in two different vibrational states results in equal and opposite contributions to the level energies, and thus to transition frequencies. The resonance effects are readily visible in simple frequency difference plots between excited state transitions and their ground state counterparts. Such plots are not critically dependent on the progress of the fit and, when made as a function of J, allow matching characteristic mirror image resonance spikes, typically belonging to higher K_a transitions in the lower vibrational state and lower K_a transitions in the upper state. This is due to the requirement for the rotational levels in the two vibrational states at the same value of J to be matched in energy.

The difference ΔK_a for perturbed transitions in the two vibrational states is a useful measure of the type of resonance and Fig. 7 highlights a complication arising from the level degeneracies prevalent in benzonitrile. It turns out that this gives rise to a $\Delta K_a = 2$ perturbation degenerate with a $\Delta K_a = 4$ perturbation, as marked in the figure. These two perturbation series are distinct since they originate from separate pairs of matrices of the Hamiltonian. Fig. 7 also allows reading off the magnitude of the perturbation at the maximum, which is close to ±360 MHz for the $J'' = 119$ transitions and would be immensely challenging to assign without using the proper coupling terms.

Once a fit is moderately advanced, it is possible to obtain an overview of the complete perturbation landscape between the two vibrational states, as shown in Fig. 8. The contour plot is, in this case, based on values of mixing coefficients for individual energy levels, which are available in the output of the SPCAT program. The plots in Fig. 7 can be seen to correspond to vertical cuts

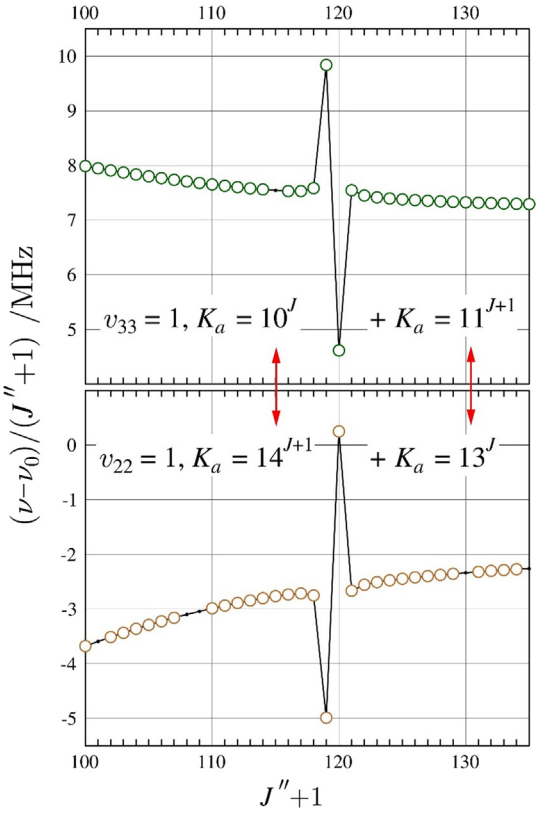

Fig. 7. Resonance plots depicting degenerate $\Delta K_a = 2$ and $\Delta K_a = 4$ local perturbations between v_{22} and v_{33}. Measured transitions are represented by open circles and predictions from the final coupled fit are in black. The two plots have identical dispersion along the vertical axis and their exact mirror image correspondence confirms the K_a assignment of the resonance partners.

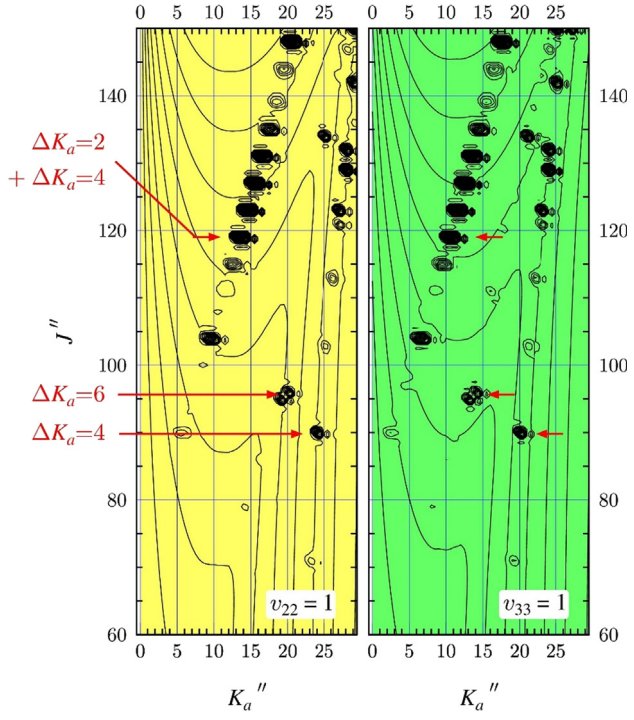

Fig. 8. Contour plot depicting the coupling landscape between rotational levels in $v_{22} = 1$ and $v_{33} = 1$ vibrational states. The mapped values are $(1 - P_{mix})$ where P_{mix} is the mixing coefficient of a given vibration-rotation energy level. Resonances between levels in the two vibrational states are apparent as matching, similarly shaped islands along the horizontal direction (same J) but differing in the values of K_a (see text). Red arrows indicate examples of several distinct types of resonances between the two vibrational states. The two prominent diagonal sequences appear to be resonances for $\Delta K_a = 3$, but are in fact sums of $\Delta K_a = 2$ and $\Delta K_a = 4$ resonances, hence the horizontally elongated resonance islands. (For interpretation of the references to color in this figure legend, the reader is referred to the web version of this article.)

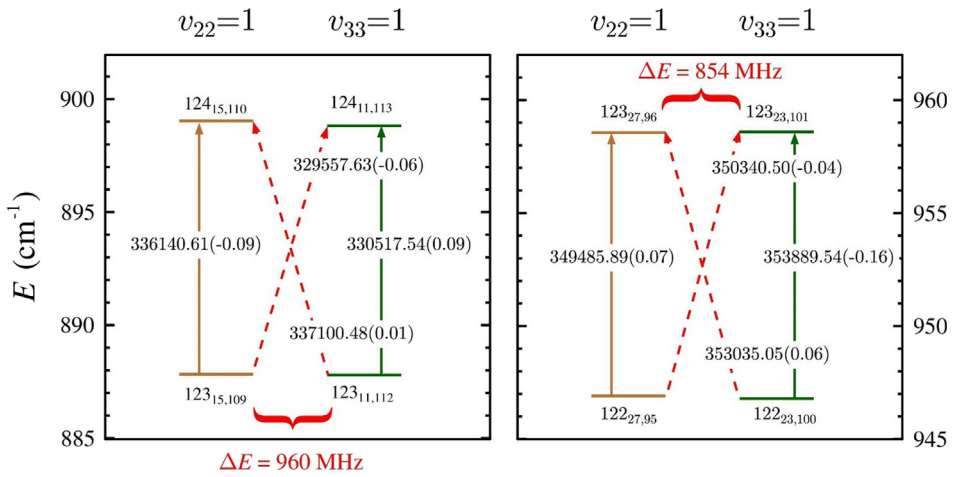

Fig. 9. Energy diagrams illustrating the origin of representative nominal rotation-vibration transitions between v_{22} = 1 and v_{33} = 1 vibrational states. The vertical arrows mark the standard $^{a}R_{0,1}$ pure rotation transitions, while the slanted arrows indicate the transitions enabled by strong mixing between rotational levels in the two vibrational states. The marked transition frequencies are in MHz and the quantities in parentheses are obs.–calc. values from the final fit. The ΔE values in red are the energy differences between the most perturbed levels. (For interpretation of the references to color in this figure legend, the reader is referred to the web version of this article.)

through the contour plot in Fig. 8, made at centers of the islands of perturbation matched along the J coordinate. It is easily seen that resonances are most frequent above J = 100 and this region fortunately turns out to be well covered by the 250–360 GHz spectral segment. The dominant series of resonances is in the form of the prominent diagonal chains of islands extending from bottom left to top right. These islands result from the combined ΔK_a = 2 and ΔK_a = 4 (ΔK_c = 3) rule and the effect of this degeneracy, visible in Fig. 8, is to elongate the perturbation islands along the K_a coordinate so that their apparent centers are separated by ΔK_a = 3. Non-degenerate, ΔK_a = 4 and ΔK_a = 6 (ΔK_c = 5) perturbations are also possible and examples are indicated in Fig. 8.

A near-final fit also facilitated a search for nominal interstate transitions. These are transitions between rotational levels in the two vibrational states, involving transitions at the perturbation maxima, such as those in Fig. 7. Perturbation induces mixing within pairs of such levels with the result illustrated for two different examples in Fig. 9. In each case, there is a pair of levels separated by less than 1 GHz, and their mixing allows observation not only to the standard (vertical) rotational transitions within each vibrational state, but also to the interstate (diagonal) transitions between the vibrational states. The interstate transitions are normally forbidden. In these two cases, their intensity is comparable to those of the pure rotational transitions, although it decreases rapidly with a decrease in level mixing. There are, however, useful precautions that can be taken in order to avoid spurious assignment of often weak lines. Since mixing gives rise to both (v_{33} = 1) ← (v_{22} = 1) and (v_{22} = 1) ← (v_{33} = 1) transitions of equal intensity, the most robust solution is to measure only such "matched pairs". An additional check of the procedure is that the average of nominal interstate transition frequencies is expected to be identical to the average of the corresponding intrastate transition frequencies. A table of these interstate transitions with their corresponding intrastate transitions, their frequencies, and the average frequency analysis is provided in the Supplementary Material. We have been able to identify and include in the data set a total of 11 such pairs, and their frequencies are fitted to within experimental accuracy, helping to precisely define the energy difference between the two studied vibrational states to microwave accuracy.

4.2.2. Comparison with computations

The key results from anharmonic force-field calculations to compare with experiment are vibrational changes in rotational constants. The respective values are listed in Table 3, although some care is necessary in making the comparison. There is excellent agreement between experiment and both computations concerning vibrational changes in B and C rotational constants for the two vibrational states. On the other hand, there is apparent disagreement in the values of ($A_v - A_0$). The coupled fit shows that there is practically no change from the ground state, while computations predict large, opposed sign changes for the two states. It should be realized, however, that computations include contributions from Eqs. (2) and (3), which are explicitly taken out in the coupled fit by use of the G_a parameter [32]. Since these Coriolis contributions are quite symmetric, however, the mean of the sum of the calculated vibrational changes can be compared with the well-determined experimental value derived from ($A_{22} + A_{33}$)/2 in Table 2. This comparison turns out to be quite

Table 3
Comparison of experimental and computed vibration-rotation interaction constants (negative α_i values) in rotational constants for v_{22} = 1 and v_{33} = 1 excited vibrational states of benzonitrile.[a]

	v_{22} = 1	v_{33} = 1	Mean[b]
Expt. deperturbed			
$A_v - A_0$ (MHz)	−0.8(20)	−0.5(20)	−0.6(1.4)
$B_v - B_0$ (MHz)	1.74538(5)	2.85016(5)	
$C_v - C_0$ (MHz)	1.83409(5)	0.81882(5)	
Calc. B3LYP			
$A_v - A_0$ (MHz)	−129.85	128.47	−0.69
$B_v - B_0$ (MHz)	1.7101	2.7187	
$C_v - C_0$ (MHz)	1.8043	0.7678	
Calc. CCSD			
$A_v - A_0$ (MHz)	−158.06	156.89	−0.59
$B_v - B_0$ (MHz)	1.6720	2.7375	
$C_v - C_0$ (MHz)	1.7712	0.7778	
Expt. effective[c]			
$A_v - A_0$ (MHz)	−160.13(2)	159.14(2)	−0.49(1)
$B_v - B_0$ (MHz)	1.6102(5)	2.7739(4)	
$C_v - C_0$ (MHz)	1.9631(5)	0.9023(3)	
Estimated Coriolis term[d]			
$A_v - A_0$ (MHz)	−137.8(51)	137.7(5.1)	−0.05(359)

[a] By the convention used in the CFOUR program, the numbers shown are the α values.
[b] The average of values for the two states, equal to $[(A_{22} - A_0) + (A_{33} - A_0)]/2$.
[c] Obtained by refitting the complete two-state data set on setting all coupling parameters to zero, to a cutoff parameter of 3σ, see text.
[d] Estimated using Eqs. (2) and (3) and the experimental value of $\zeta^{a}_{22,33}$.

Table 4
Comparison of selected experimental and calculated vibrational parameters for v_{22} = 1 and v_{33} = 1 excited vibrational states of benzonitrile.

	Expt.	B3LYP	CCSD
v_{22} (cm^{-1})	141[a]	145.0 (144.2)[b]	147.2 (155.5)[b]
v_{33} (cm^{-1})	163[a]	168.9 (168.1)[b]	166.9 (169.2)[b]
ΔE (cm^{-1})	19.108185(7)	23.9 (23.9)[b]	19.7 (13.9)[b]
$\zeta^a_{22,33}$	0.841(7)	0.8268	0.8300
Δ_i (v_{22} = 1) (uÅ^2)	−2.8559(4)[c]	−2.284	−2.726
Δ_i (v_{33} = 1) (uÅ^2)	2.8018(3)[c]	2.397	2.744

[a] Ref. [20].
[b] Values given for harmonic and (anharmonic) treatment of vibrations.
[c] Calculated from rotational constants from the effective fit.

satisfactory. We can also attempt to derive effective values of experimental rotational constants by foregoing the interstate coupling, and fitting two single-state asymmetric rotor Hamiltonian models to the data set by using a cutoff criterion in obs. − calc. frequencies in order to reject the most perturbed transitions. This procedure is not completely unambiguous as it gives slightly differing results depending on the type of "annealing" from the coupled state fit, but the specimen result listed in Table 3 is reasonably close to the direct values from the computations.

Table 4 compares experiment and computation concerning the remaining vibrational quantities. The precise energy difference of 19.108185(7) cm^{-1} between the two vibrational states determined presently cannot be compared to data of high-resolution vibration-rotation spectroscopy, although it is consistent with the available low resolution infrared values [20] and with computational predictions. The current coupled-cluster or DFT values of $\zeta^a_{22,33}$ (0.8300 and 0.8268, respectively) are both excellent estimates of the experimentally determined value ($\zeta^a_{22,33}$ = 0.841(7)). Both calculations differ from experiment by only ~2%, although we should note that $\zeta^a_{22,33}$ is actually a harmonic force field quantity, and a much more rudimentary MP2/6-31G(d,p) calculation delivers an equally acceptable $\zeta^a_{22,33}$ = 0.8266. Finally, the calculated values of inertial defect for the two excited states differ considerably from the very small value for the ground state, but compare well with those derived from the effective fit made in Table 3, with a marked preference for the coupled-cluster result.

5. Conclusions

In this paper, we report the results of extensive measurements on a broadband rotational spectrum of benzonitrile. The spectrum was newly recorded with the use of several different mm-wave spectrometers and around 3000 rotational transitions have been measured in the ground state and in each of the two lowest excited vibrational states. A global single-state fit of all available data is reported for the ground state, while transitions in the newly assigned v_{22} = 1 and v_{33} = 1 states revealed multiple effects of interstate Coriolis perturbations, requiring the use of a two-state coupled fit. We have been able to identify and to measure many level-crossing resonances for quantum number value differences ΔK_a = 2, 4, and 6 between the two excited states based on predictions of vibration-rotation interaction constants from anharmonic force field calculations, and the use of dedicated graphical techniques of analysis. The final experimental results benchmark the usefulness of anharmonic computations for a molecule of this size. Prediction of sextic centrifugal distortion constants for the ground state was found to be at a useful average 15.5% accuracy for the five best determined constants. The calculated vibrational changes in rotational constants also turned out to be sufficiently precise for spectroscopic analysis, especially when comparing the values associated with the rotational axis involved in the Coriolis perturbation (*a* axis). The final two-state fit was sufficiently accurate to enable measurement of several nominal interstate transitions between v_{22} = 1 and v_{33} = 1 accessible due to state mixing. The present work reinforces previous results [32,34], in suggesting that a pair of strongly coupled lowest excited vibrational states is a generic feature of small aromatic molecules. The spectra reported in this work lay the foundation for future mm-wave searches for benzonitrile in the ISM.

Acknowledgments

We gratefully acknowledge funding from the National Science Foundation for support of this project (NSF-1664912) and for support of shared Departmental computing resources (NSF-CHE-0840494).

Declarations of interest

None.

Appendix A. Supplementary material

Supplementary data associated with this article can be found, in the online version, at https://doi.org/10.1016/j.jms.2018.06.004.

References

[1] J. Cernicharo, A.M. Heras, A.G.G.M. Tielens, J.R. Pardo, F. Herpin, M. Guelin, L.B. F.M. Waters, Infrared space observatory's discovery of C_4H_2, C_6H_2, and benzene in CRL 618, Astrophys. J. 546 (2001) L123–L126.
[2] S.B. Charnley, Y.-J. Kuan, H.-C. Huang, O. Botta, H.M. Butner, N. Cox, D. Despois, P. Ehrenfreund, Z. Kisiel, Y.-Y. Lee, A.J. Markwick, Z. Peeters, S.D. Rodgers, Astronomical searches for nitrogen heterocycles, Adv. Space Res. 36 (2005) 137–145.
[3] Y.-J. Kuan, C.-H. Yan, S.B. Charnley, Z. Kisiel, P. Ehrenfreund, H.-C. Huang, A search for interstellar pyrimidine, Mon. Not. R. Astron. Soc. 345 (2003) 650–656.
[4] P. Thaddeus, J.M. Vrtilek, C. Gottlieb, Laboratory and astronomical identification of cyclopropenylidene, C_3H_2, Astrophys. J. 299 (1985) L63–L66.
[5] P. Cox, R. Guesten, C. Henkel, Observations of cyclopropenylidene in the diffuse interstellar medium, Astron. Astrophys. 206 (1988) 108–116.
[6] J.M. Hollis, A.J. Remijan, P.R. Jewell, F.J. Lovas, Cyclopropenone (*c*-H_2C_3O): a new interstellar ring molecule, Astrophys. J. 642 (2006) 933–939.
[7] K. Wohlfart, M. Schnell, J.-U. Grabow, J. Küpper, Precise dipole moment and quadrupole coupling constants of benzonitrile, J. Mol. Spectrosc. 247 (2008) 119–121.
[8] H.S.P. Müller, S. Thorwirth, D.A. Roth, G. Winnewisser, The cologne database for molecular spectroscopy, CDMS, Astron. Astrophys. 370 (2001) L49–L52.
[9] B.A. McGuire, A.M. Burkhardt, S.V. Kalenskii, C.N. Shingledecker, A.J. Remijan, E. Herbst, M.C. McCarthy, Detection of the aromatic molecule benzonitrile (*c*-C_6H_5CN) in the interstellar medium, Science 359 (2018) 202–205.
[10] S.V. Kalenskii, Possible detection of interstellar benzonitrile, in: I. Zinchenko, P. Zemlyanukha (Eds.), Proceedings of the Russian-Indian Workshop on Radio Astronomy and Star Formation, October 10–12, 2016, Institute of Applied Physics RAS, 2017, pp. 43–50.
[11] N. Kaifu, M. Ohishi, K. Kawaguchi, S. Saito, S. Yamamoto, T. Miyaji, K. Miyazawa, S.-I. Ishikawa, C. Noumaru, S. Harasawa, M. Okuda, H. Suzuki, A 8.8-50 GHz complete spectral line survey toward TMC-1. Part 1. Survey data, Publ. Astron. Soc. Jpn. 56 (2004) 69–173.
[12] G. Wlodarczak, J. Burie, J. Demaison, K. Vormann, A.G. Császár, The rotational spectrum of benzonitrile: experimental and theoretical determination of the quartic centrifugal distortion constants, J. Mol. Spectrosc. 134 (1989) 297–304.
[13] G. Erlandsson, Microwave spectrum of benzonitrile, J. Chem. Phys. 22 (1954) 1152.
[14] D.J.R. Lide, Microwave spectrum and structure of benzonitrile, J. Chem. Phys. 22 (1954) 1577–1578.
[15] B. Bak, D. Christensen, W.B. Dixon, L. Hansen-Nygaard, J. Rastrup-Andersen, Benzene ring distortion by one substituent. Microwave determination of the complete structure of benzonitrile, J. Chem. Phys. 37 (1962) 2027–2031.
[16] J. Casado, L. Nygaard, G.O. Sørensen, Microwave spectra of isotopic benzonitriles. Refined molecular structure of benzonitrile, J. Mol. Struct. 8 (1971) 211–224.

[17] E. Fliege, G. Bestmann, R. Schwarz, H. Dreizler, Quadrupole coupling in benzonitrile. An application of microwave Fourier transform spectroscopy, Z. Naturforsch., A 36A (1981) 1124–1125.
[18] K. Vormann, U. Andresen, N. Heineking, H. Dreizler, Quadrupole hyperfine structure in the rotational spectrum of benzonitrile, Z Naturforsch., A 43 (1988) 283–284.
[19] B. Bak, J.T. Nielsen, Infrared absorption spectra of benzonitrile and its mono-deuteriated derivatives. Tentative assignments of fundamentals, Z Elektrochem. Angew. Phys. Chem. 64 (1960) 560–562.
[20] J.H.S. Green, D.J. Harrison, Vibrational spectra of benzene derivatives—XVII. Benzonitrile and substituted benzonitriles, Spectrochim. Acta, Part A 32 (1976) 1279–1286.
[21] A.G. Császár, G. Fogarasi, Scaled quantum mechanical (SQM) force field and theoretical vibrational spectrum for benzonitrile, Spectrochim. Acta, Part A 45 (1989) 845–854.
[22] U. Dahmen, W. Stahl, H. Dreizler, The rotational spectrum of the benzonitrile-argon van der Waals complex, Ber. Bunsen – Ges. Phys. Chem. 98 (1994) 970–974.
[23] H.D. Rudolph, J. Demaison, A.G. Csaszar, Accurate determination of the deformation of the benzene ring upon substitution: equilibrium structures of benzonitrile and phenylacetylene, J. Phys. Chem. A 117 (2013) 12969–12982.
[24] B.N. Khare, C. Sagan, J.E. Zumberge, D.S. Sklarew, B. Nagy, Organic solids produced by electrical discharge in reducing atmospheres: tholin molecular analysis, Icarus 48 (1981) 290–297.
[25] N. Balucani, O. Asvany, L.C.L. Huang, Y.T. Lee, R.I. Kaiser, Y. Osamura, H.F. Bettinger, Formation of nitriles in the interstellar medium via reactions of cyano radicals, CN($X_2\Sigma^+$), with unsaturated hydrocarbons, Astrophys. J. 545 (2000) 892.
[26] P.M. Woods, T.J. Millar, A.A. Zijlstra, H. Eric, The synthesis of benzene in the proto-planetary nebula CRL 618, Astrophys. J. 574 (2002) L167.
[27] D.E. Woon, Modeling chemical growth processes in Titan's atmosphere: 1. Theoretical rates for reactions between benzene and the ethynyl (C_2H) and cyano (CN) radicals at low temperature and pressure, Chem. Phys. 331 (2006) 67–76.
[28] D.S.N. Parker, R.I. Kaiser, O. Kostko, T.P. Troy, M. Ahmed, B.-J. Sun, S.-H. Chen, A. H.H. Chang, On the formation of pyridine in the interstellar medium, Phys. Chem. Chem. Phys. 17 (2015) 32000–32008.
[29] K.B. Jefferts, A.A. Penzias, R.W. Wilson, Observation of the CN radical in the Orion Nebula and W51, Astrophys. J. 161 (1970) L87.
[30] S.E. Malek, J. Cami, J. Bernard-Salas, The rich circumstellar chemistry of SMP LMC 11, Astrophys. J. 744 (2012) 16.
[31] D.A. García-Hernández, P. García-Lario, J. Cernicharo, D. Engels, J.V. Perea-Calderón, Transitory O-rich chemistry in heavily obscured C-rich post-AGB stars, J. Phys. Conf. Ser. 728 (2016) 052003.
[32] Z. Kisiel, A. Kraśnicki, The millimetre-wave rotational spectrum of phenylacetylene, J. Mol. Spectrosc. 262 (2010) 82–88.
[33] B.J. Esselman, B.K. Amberger, J.D. Shutter, M.A. Daane, J.F. Stanton, R.C. Woods, R.J. McMahon, Rotational spectroscopy of pyridazine and its isotopologs from 235–360 GHz: equilibrium structure and vibrational satellites, J. Chem. Phys. 139 (2013) 224304.
[34] O. Pirali, Z. Kisiel, M. Goubet, S. Gruet, M.A. Martin-Drumel, A. Cuisset, F. Hindle, G. Mouret, Rotation-vibration interactions in the spectra of polycyclic aromatic hydrocarbons: quinoline as a test-case species, J. Chem. Phys. 142 (2015) 104310.
[35] I. Medvedev, M. Winnewisser, F.C. De Lucia, E. Herbst, E. Białkowska-Jaworska, L. Pszczółkowski, Z. Kisiel, The millimeter- and submillimeter-wave spectrum of the *trans–gauche* conformer of diethyl ether, J. Mol. Spectrosc. 228 (2004) 314–328.
[36] Z. Kisiel, L. Pszczółkowski, B.J. Drouin, C.S. Brauer, S. Yu, J.C. Pearson, I.R. Medvedev, S. Fortman, C. Neese, Broadband rotational spectroscopy of acrylonitrile: vibrational energies from perturbations, J. Mol. Spectrosc. 280 (2012) 134–144.
[37] Z. Kisiel, L. Pszczółkowski, I.R. Medvedev, M. Winnewisser, F.C. De Lucia, E. Herbst, Rotational spectrum of *Trans-Trans* diethyl ether in the ground and three excited vibrational states, J. Mol. Spectrosc. 233 (2005) 231–243.
[38] Z. Kisiel, in: J. Demaison et al. (Eds.), Spectroscopy from Space, Kluwer Academic Publishers, Dordrecht, 2001, pp. 91–106.
[39] Z. Kisiel, PROSPE—Programs for ROtational SPEctroscopy. <http://info.ifpan.edu.pl/~kisiel/prospe.htm>.
[40] H.M. Pickett, The fitting and prediction of vibration-rotation spectra with spin interactions, J. Mol. Spectrosc. 148 (1991) 371–377.
[41] J.A. Pople, M. Head-Gordon, K. Raghavachari, Quadratic configuration interaction. A general technique for determining electron correlation energies, J. Chem. Phys. 87 (1987) 5968–5975.
[42] J.F. Stanton, J. Gauss, L. Cheng, M.E. Harding, D.A. Matthews, P.G. Szalay, CFOUR, Coupled-Cluster Techniques for Computational Chemistry, a quantum-chemical program package with contributions from A.A. Auer, R.J. Bartlett, U. Benedikt, C. Berger, D.E. Bernholdt, Y.J. Bomble, O. Christiansen, F. Engel, R. Faber, M. Heckert, O. Heun, C. Huber, T.-C. Jagau, D. Jonsson, J. Jusélius, K. Klein, W.J. Lauderdale, F. Lipparini, T. Metzroth, L.A. Mück, D.P. O'Neill, D.R. Price, E. Prochnow, C. Puzzarini, K. Ruud, F. Schiffmann, W. Schwalbach, C. Simmons, S. Stopkowicz, A. Tajti, J. Vázquez, F. Wang, J.D. Watts and the integral packages MOLECULE (J. Almlöf and P.R. Taylor), PROPS (P.R. Taylor), ABACUS (T. Helgaker, H.J. Aa. Jensen, P. Jørgensen, and J. Olsen), and ECP routines by A. V. Mitin and C. van Wüllen. For the current version, see <www.cfour.de>.
[43] G.E. Scuseria, Analytic evaluation of energy gradients for the singles and doubles coupled cluster method including perturbative triple excitations: theory and applications to FOOF and Cr_2, J. Chem. Phys. 94 (1991) 442–447.
[44] T.J. Lee, A.P. Rendell, Analytic gradients for coupled-cluster energies that include noniterative connected triple excitations: application to *cis*- and *trans*-HONO, J. Chem. Phys. 94 (1991) 6229–6236.
[45] I.M. Mills, Molecular Spectroscopy: Modern Research, Academic Press, New York, 1972.
[46] J.F. Stanton, C.L. Lopreore, J. Gauss, The equilibrium structure and fundamental vibrational frequencies of dioxirane, J. Chem. Phys. 108 (1998) 7190–7196.
[47] M.J. Frisch, G.W. Trucks, H.B. Schlegel, G.E. Scuseria, M.A. Robb, J.R. Cheeseman, G. Scalmani, V. Barone, B. Mennucci, G.A. Petersson, H. Nakatsuji, M. Caricato, X. Li, H.P. Hratchian, A.F. Izmaylov, J. Bloino, G. Zheng, J.L. Sonnenberg, M. Hada, M. Ehara, K. Toyota, R. Fukuda, J. Hasegawa, M. Ishida, T. Nakajima, Y. Honda, O. Kitao, H. Nakai, T. Vreven, J.A. Montgomery Jr., J.E. Peralta, F. Ogliaro, M.J. Bearpark, J. Heyd, E.N. Brothers, K.N. Kudin, V.N. Staroverov, R. Kobayashi, J. Normand, K. Raghavachari, A.P. Rendell, J.C. Burant, S.S. Iyengar, J. Tomasi, M. Cossi, N. Rega, N.J. Millam, M. Klene, J.E. Knox, J.B. Cross, V. Bakken, C. Adamo, J. Jaramillo, R. Gomperts, R.E. Stratmann, O. Yazyev, A.J. Austin, R. Cammi, C. Pomelli, J.W. Ochterski, R.L. Martin, K. Morokuma, V.G. Zakrzewski, G.A. Voth, P. Salvador, J.J. Dannenberg, S. Dapprich, A.D. Daniels, Ö. Farkas, J.B. Foresman, J.V. Ortiz, J. Cioslowski, D.J. Fox, Gaussian 09. Gaussian, Inc., Wallingford, CT, USA, 2009.
[48] J.R. Schmidt, W.F. Polik, WebMO Enterprise. 17.0.012e ed.; WebMO, LLC., Holland, MI, USA, 2017.
[49] Z. Kisiel, E. Białkowska-Jaworska, L. Pszczółkowski, The mm-wave rotational spectrum of $CBrClF_2$ (Halon BCF): observation of a new R-type band and generalization of conditions for oblate-type band formation, J. Mol. Spectrosc. 177 (1996) 240–250.
[50] Z. Kisiel, L. Pszczółkowski, Assignment and analysis of the mm-wave rotational spectrum of trichloroethylene: observation of a new, extended ^{b}R-band and an overview of high-J, R-type bands, J. Mol. Spectrosc. 178 (1996) 125–137.
[51] J.K.G. Watson, Vibrational Spectra and Structure, Elsevier, Amsterdam, 1977.
[52] Z. Kisiel, E. Białkowska-Jaworska, R.A.H. Butler, D.T. Petkie, P. Helminger, I.R. Medvedev, F.C. De Lucia, The rotational spectrum of chlorine nitrate ($ClONO_2$) in the four lowest $n_{\nu 9}$ polyads, J. Mol. Spectrosc. 254 (2009) 78–86.